ACS POLYMERS Au
AN OPEN ACCESS JOURNAL OF THE AMERICAN CHEMICAL SOCIETY

pubs.acs.org/polymerau
Article

Structural Engineering of L-Aspartic Amphiphilic Polyesters for Enzyme-Responsive Drug Delivery and Bioimaging in Cancer Cells

Published as part of ACS Polymers Au virtual special issue "Polymer Science and Engineering in India".

Mohammed Khuddus, Utreshwar Arjun Gavhane, and Manickam Jayakannan*

Cite This: ACS Polym. Au 2024, 4, 392−404
Read Online

ABSTRACT: Design and development of amphiphilic polyesters based on bioresources are very important to cater to the ever-growing need for biodegradable polymers in biomedical applications. Here, we report structural engineering of enzyme-responsive amphiphilic polyesters based on L-amino acid bioresources and study their drug delivery aspects in the cancer cell line. For this purpose, an L-aspartic acid-based polyester platform is chosen, and two noncovalent forces such as hydrogen bonding and side-chain hydrophobic interactions are introduced to study their effect on the aqueous self-assembly of nanoparticles. The synthetic strategy involves the development of L-aspartic acid-based dimethyl ester monomers with acetal and stearate side chains and subjecting them to solvent-free melt polycondensation reactions to produce side-chain-functionalized polyesters in the entire composition range. Postpolymerization acid catalyst deprotection of acetal yielded hydroxyl-functionalized polyesters. Amphiphilicity of the polymer is carefully fine-tuned by varying the composition of the stearate and hydroxyl units in the polymer chains to produce self-assembly in water. Various drugs such as camptothecin (CPT), curcumin (CUR), and doxorubicin (DOX) and biomarkers like 8-hydroxypyrene-1,3,6-trisulfonic acid trisodium salt (HPTS), rose bengal (RB), and Nile red (NR) are successfully encapsulated in the polymer nanoparticles. Cytotoxicity of biodegradable polymer nanoparticles is tested in normal and breast cancer cell lines. The polymer nanoparticles are found to be highly biocompatible and delivered the anticancer drugs in the intracellular compartments of the cells.

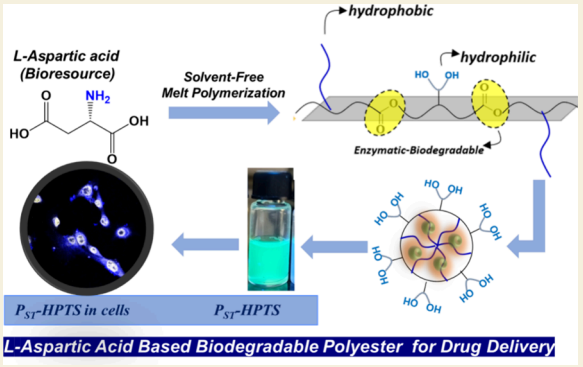

KEYWORDS: *amino acid, polyesters, melt polycondensation, polymer nanoparticles, drug delivery, biodegradable polymers*

INTRODUCTION

Polymers are emerging as indispensable components in biomedical applications, and they have become an integral part of drug delivery systems,[1−3] gene delivery vehicles,[4] tissue engineering scaffolds,[5,6] and antimicrobial agents.[7,8] Synthetic polymers gained significant importance because of their tunable properties, including biocompatibility, biodegradability, and versatility in molecular design, which made them highly attractive for addressing diverse biomedical challenges.[9−11] Among the myriad classes of polymers, biodegradable variants hold particular significance, offering controlled degradation that aligns with the dynamic needs of biological systems.[12−15] These polymers not only mitigate concerns related to long-term accumulation and toxicity but also facilitate the controlled release of therapeutic agents, thereby enhancing efficacy and minimizing adverse effects.[16−18] Within the domain of biodegradable polymers, those derived from natural resources hold immense promise; notably, the polymers synthesized from L-amino acids via ring-opening polymerization (ROP) have garnered considerable attention owing to their inherent biocompatibility and structural resemblance to biological macromolecules.[19−23] This includes the development of synthetic amphiphilic polypeptides mimicking the natural-protein-type self-assemblies under physiological conditions.[24] To address the limitation in the biodegradation aspects and broaden the scope of biomedical applications of L-amino acid bioresources, alternative non-peptide analogues such as poly(ester amides),[25−27] polycarbonates,[28] poly(ester urea urethanes),[29] poly(disulfide urethanes),[30] and poly(acetal urethanes)[31] have been explored. Our research has focused on the development of new classes of polyesters, polyurethanes, and poly(ester-urethanes) from L-amino acid bioresources.[32−42] These polymers have undergone

Received: February 25, 2024
Revised: July 10, 2024
Accepted: July 10, 2024
Published: July 17, 2024

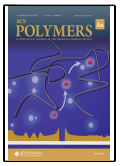

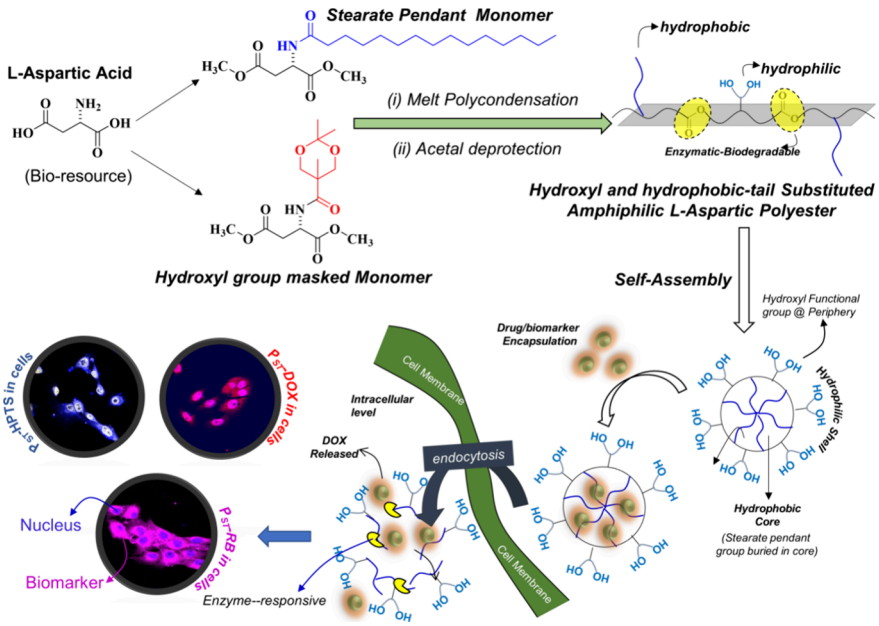

Figure 1. Solvent-free melt polycondensation strategy for the development of hydroxyl-functionalized aliphatic polyesters containing stearate pendants and their enzyme-responsive drug delivery in cancer cells.

rigorous scrutiny for drug delivery applications both *in vitro* and *in vivo*.[43] Polymers bearing hydroxyl functional groups have a special place in the biomaterial arena due to their unique ability to anchor desired targeting agents and drug molecules to improve the efficacy of the drug delivery aspects.[44,36] Unfortunately, these functional groups interfere in the polymerization protocols, and therefore, an additional masking strategy is required to overcome this limitation. Functional polyesters are typically produced by employing multitask monomers in the polymerization step and employing an appropriate deprotection strategy to restore the desired functional units in the postpolymerization step.[45−50] In our continuous effort to explore L-amino acid bioresources for biomedical applications, here, efforts have been taken to structurally engineer biodegradable aliphatic polyesters, for the first time, having hydroxyl functional groups as the hydrophilic handle and side-chain stearate pendant groups as the hydrophobic handle. It is very important to mention that hydroxyl-functionalized polyesters are relatively rarely reported in the literature due to the synthetic complexity; thus, this new effort really opens up new opportunities to program the polyester amphiphilicity for aqueous self-assembly. By controlling the composition of hydroxyl groups and hydrophobic side chains, the self-assembly aspects of the aliphatic polyesters based on L-aspartic acid could be programmed for drug and biomarker delivery in cancer cells, and this new strategy is shown in Figure 1.

The present approach employs hydroxyl functional groups for a hydrophilic content and stearate chains for a hydrophobic content to bring appropriate amphiphilicity to enhance their drug or biomarker encapsulation in the nanocavity. For this purpose, L-aspartic acid was converted to dimethyl ester monomers containing acetal and stearate pendant groups. Employing a melt polycondensation strategy with L-aspartic dimethyl ester and 1,12-dodecane diol monomers facilitated the synthesis of acetal-functionalized polymers bearing various compositions of stearate pendant groups. The solid-state packing was studied in detail by thermal transitions such as melting and crystallization processes that revealed that the introduction of side-chain stearate is a very crucial factor for introducing semicrystallinity in the sluggish amorphous backbone. Postpolymerization deprotection of the acetal side chains under acidic conditions yielded hydroxyl-functionalized polymers with stearate pendant groups, and the amphiphilic balance resulted in the stable aqueous nanoparticle formulations. The enzyme responsiveness of the L-aspartic acid aliphatic polyester backbone renders biodegradability to release the loaded cargos at the intracellular compartment; the concept is illustrated in Figure 1. Anticancer drugs and biomarkers were encapsulated in the nanoparticles, and these polymer nanoparticles were found to be less than 250 nm in size with a drug loading content (DLC) varying from 1 to 12%. The drug-loaded nanoparticles underwent enzyme-responsive release under physiological conditions. Studies on the cellular uptake of the polymer nanoparticles demonstrated their effective internalization of cargo molecules into the cancer cell cytoplasm. This comprehensive study demonstrates that bioresources such as L-amino acid-based polymers may be used as a nanocarrier for drug delivery and bioimaging in cancer cells.

EXPERIMENTAL SECTION

Materials and Methods

The following substances were obtained from Sigma-Aldrich chemicals: 1,12-dodecane diol, 2,2-bis(hydroxymethyl)propionic acid, *p*-toluene sulfonic acid, *N*,*N*′-dicyclo-hexyl-carbodiimide, acid, and titanium tetrabutoxide $Ti(OBu)_4$. The substances were employed directly without additional purification. The following items were purchased locally and purified before use: L-aspartic acid, thionyl chloride, methanol, acetone, dimethyl aminopyridine, dichloromethane, ethyl acetate, PET ether, silica gel, tetrahydrofuran, dimethyl sulfoxide, and toluene, among other solvents. The acetal monomer M-AC and stearic monomer M-ST were synthesized following our earlier reports.[36,37] These monomers were polymerized by melt polycondensation along with 1,12-dodecane diol as reported earlier to yield homopolyesters P-ST and P-AC.[36,37]

https://doi.org/10.1021/acspolymersau.4c00013
ACS Polym. Au 2024, 4, 392−404

Biological Procedure

To maintain the cell culture, complete media were prepared by mixing DMEM media with 10% FBS and 1% penicillin and streptomycin solution. The cell culture MCF-7 and WT-MEF cells were maintained in a 37 °C incubator with 5% CO_2.

Nuclear Magnetic Resonance

A Jeol NMR spectrophotometer operating at 400 MHz is a high-resolution instrument used for recording nuclear magnetic resonance (NMR) spectra. In NMR experiments, TMS (tetramethylsilane) was used as an internal standard to reference chemical shifts. $CDCl_3$ (deuterated chloroform) was used as a solvent for NMR experiments.

Size Exclusion Chromatography (SEC)

Size exclusion chromatography (SEC) was performed with THF as an eluent; polystyrene standards were employed in SEC analysis as a reference for estimating the molecular weight of polymers. The Viscotek VE series instruments mentioned used components in SEC setups, with the pump facilitating solvent flow, the RI (refractive index) detector measuring changes in the refractive index, and the UV/vis detector detecting changes in absorbance at specific wavelengths.

Thermal Characterization

A PerkinElmer thermal analyzer STA 6000 is a thermal analysis instrument used for studying the thermal properties of materials. Thermal decomposition and stability of polymers can be investigated by subjecting them to controlled heating under an inert atmosphere. Differential scanning calorimetry (DSC) is a technique used to measure changes in heat capacity as a function of temperature.

Size of the Polymer Nanoparticles

Dynamic light scattering (DLS) is a technique used to measure the size distribution of particles in solution based on the fluctuations in the intensity of scattered light. A Nano ZS-90 apparatus from Malvern Instruments is a commonly used instrument for DLS measurements. The size and shape of the nanoparticles were also confirmed by AFM and HR-TEM. For AFM microscopy imaging, the samples were drop cast on a silicon wafer and dried over a period of 1 week; then, samples were analyzed using a Vecco Nanoscope IV. While in the case of HR-TEM, the samples were drop cast on a Formvar-coated copper grid and dried over a period of 1 week and analyzed using TEM; images were recorded using a Tecnai-300 instrument.

UV−Vis Spectroscopy

UV−vis spectroscopy is a technique used to measure the absorption of light by a substance (chromophore) as a function of the wavelength. Absorption spectra were recorded using a PerkinElmer Lambda 45 UV−vis spectrophotometer.

Fluorescence Spectroscopy

Fluorescence spectroscopy is a technique used to study the emission of light by a substance following excitation with light of a specific wavelength. An SPEX Fluorolog Horiba Jobin Yvon fluorescence spectrophotometer mentioned is a specialized instrument used for measuring fluorescence spectra with the ability to excite samples with a 450 W xenon lamp and detect emitted fluorescence over a range of wavelengths.

Lyophilization, or freeze-drying, is a process used to remove water from samples while preserving their structure and activity. A Christ Alpha 1-2 LDplus is a model lyophilizer used in laboratory settings.

The Cell Viability Assay

A Varioskan Flash device is a microplate reader used for measuring absorbance or fluorescence in multiwell plates in the MTT assay. It can be used for quantifying the concentration of substances in solution such as the formazan concentration mentioned in the context of cell viability assays.

Bioimaging Experiments

Fixed-cell experiments involve treating cells with various compounds or nanoparticles and then fixing them in place to visualize specific cellular structures or processes. The LSM710 confocal microscope mentioned is a sophisticated imaging system that uses lasers of different wavelengths to excite fluorescently labeled samples, allowing for high-resolution imaging of cellular components. The 63× lens mentioned refers to the magnification level of the objective lens used for capturing images at a high resolution.

Flow Cytometry Experiments

A BD LSRFortessa SORP cell analyzer is a flow cytometer used for analyzing cell populations by measuring the physical and chemical characteristics of the cells in a fluid suspension. It is equipped with multiple lasers and detectors, allowing for the simultaneous detection of various fluorophores in flow cytometry experiments.

Synthesis of the Random Copolymer P-ST_{10}

The general procedure for the synthesis of a random copolymer is described in detail for the P-ST_{10}. The molar ratio of the two monomers M-AC (0.7 g, 1.8 mmol) and M-ST (0.10 g, 0.2 mmol) was kept as 90:10, respectively, along with the molar ratio of 100% of 1,12-dodecane diol (0.5 g, 2.0 mmol). M-Ac and M-ST were taken in a clean polymerization tube along with 1,12-dodecane diol, and the polymerization mixture was melted at 140 °C. The $Ti(OBu)_4$ catalyst (1 mol %) was added. The polymerization was performed in two steps: (i) in the first step, the polymerization mixture was subjected to 4 h of continuous nitrogen purging, and (ii) in the second step, the polymerization mixture was subjected to 0.01 mbar stirring under vacuum for 2 h at the same temperature. The polymer was purified by precipitation in methanol. Yield = 1.27 g (98%). ^{1}H NMR (400 MHz, chloroform-*d*): δ ppm 8.02 (1 H, d), 4.86 (1 H, m), 4.12 (2 H, m), 4.04 (2 H, t), 3.91 (2 H, m), 3.75 (2 H, dd), 3.00 (1 H, m), 2.86 (1 H, dd), 1.57 (5 H, m), 1.42 (6 H, m), 1.24 (20 H, br s), 0.99 (3 H, s). ^{13}C NMR (101 MHz, chloroform-*d*): δ ppm 174.3, 170.8, 170.4, 170.4, 98.1, 76.7, 76.4, 67.5, 66.4, 65.6, 65.5, 65.4, 64.9, 64.7, 64.7, 62.4, 48.3, 48.2, 48.0, 47.5, 39.7, 36.0, 35.9, 35.7, 32.3, 31.5, 30.4, 29.2, 29.1, 29.0, 28.9, 28.8, 28.8, 28.7, 28.1, 28.0, 27.9, 25.4, 25.3, 25.1, 22.2, 18.1, 17.2, 17.0, 13.7.

General Procedure for Deprotection of Acetal-Functionalized Copolymers

The copolymer was taken in a clean round-bottom flask to which dichloromethane was added under the ice-cold condition; trifluoracetic acid was added dropwise to the reaction mixture. After 15 min, water was added to the reaction mixture. The reaction was carried out for 2 h. After 2 h, trifluoracetic acid was removed from the reaction mixture using a rotary evaporator along with dichloromethane. The polymer was further purified by the dialysis method in water, and after dialysis, water was removed by lyophilization and characterized by NMR spectroscopy.

Synthesis of PST_{10}-OH

PST_{10} (0.5 g, 1.0 mmol) and trifluoracetic acid (1.0 mL, 13.0 mmol) were taken with a similar procedure as mentioned in the general procedure for deprotection of acetal-functionalized copolymers. Yield = 0.45 g (90%). ^{1}H NMR (400 MHz, chloroform-*d*): δ ppm 1.09 (s, 1 H), 1.28 (br s, 15 H), 1.57 (br s, 4 H), 2.63 (s, 3 H), 2.87 (br s, 1 H), 3.00 (br s, 1 H), 3.64 (s, 2 H), 3.78 (br s, 2 H), 4.07 (br s, 1 H), 4.16 (br s, 1 H), 4.88 (br s, 1 H), 7.02 (br s, 1 H), 7.11 (br s, 1 H). ^{13}C NMR (101 MHz, chloroform-*d*): δ ppm −0.03, 17.37, 25.69, 28.45, 29.14, 29.37, 29.43, 29.50, 29.54, 32.74, 36.05, 48.69, 63.06, 65.46, 66.27, 76.69, 77.31, 113.98, 126.39, 127.60, 131.27, 132.70, 171.04.

Self-Assembly and Dye Loading Studies

The polymer was self-assembled in an aqueous medium. It was carried out by using a dialysis method. Five mg of the polymer was weighed and dissolved into 2.0 mL of dimethyl sulfoxide; then, the solution was transferred to a dialysis tube (semipermeable membrane of 1000 Da) and dialyzed against water. Nile red was loaded by following a similar protocol where 5.0 mg of the polymer was dissolved in 2.0 mL of dimethyl sulfoxide; then, 100 μL of Nile red solution was added to it. Three mL of water was added to the solution. This solution was

https://doi.org/10.1021/acspolymersau.4c00013
ACS Polym. Au 2024, 4, 392−404

Scheme 1. (a) Synthesis of Acetal and Stearate L-Aspartic Acid Dimethyl Ester Monomers, (b) Melt Polycondensation for Synthesis of Homopolymers P-Ac and P-ST, and (c) Synthesis of Copolymers P-ST$_X$

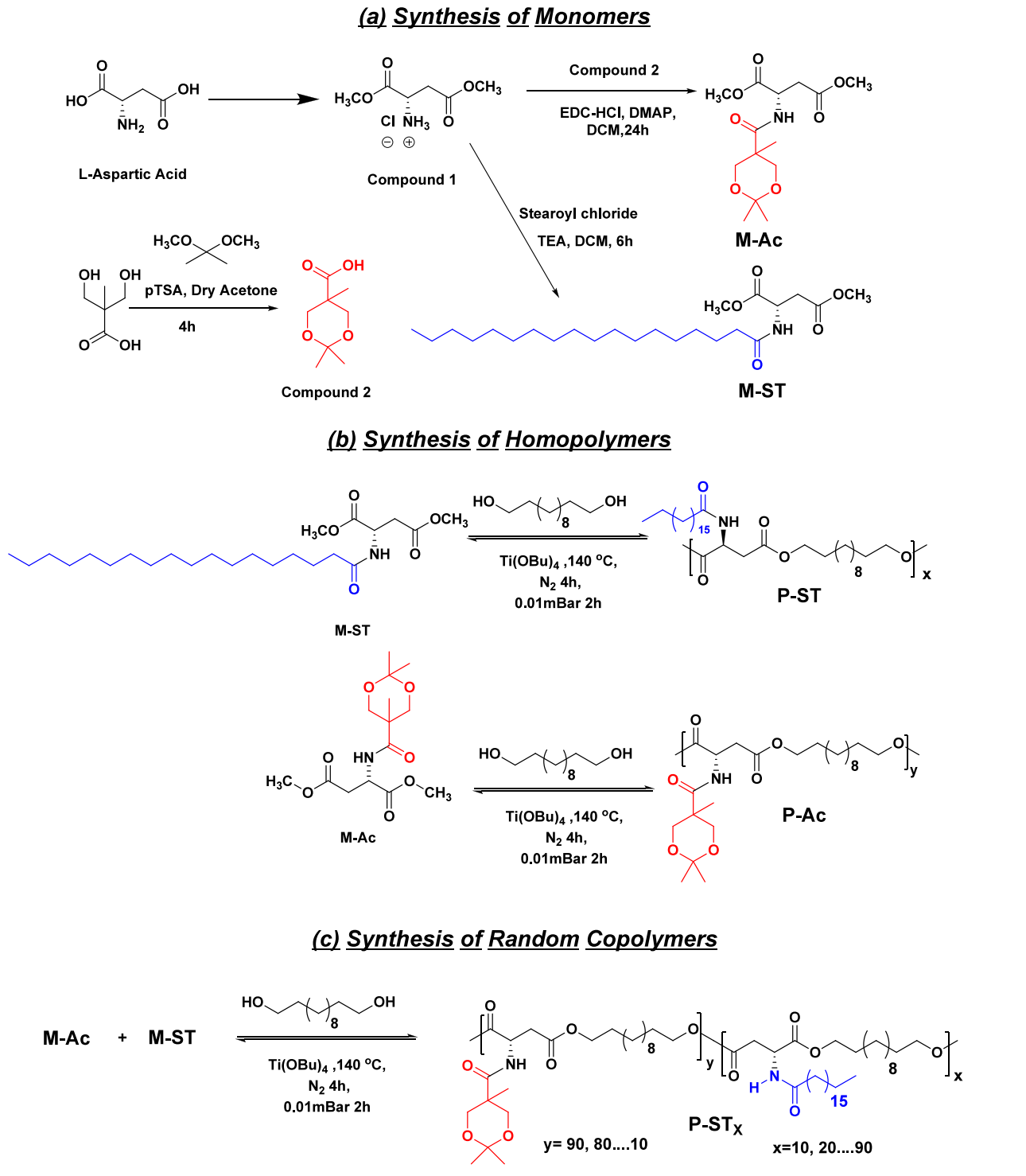

dialyzed using Milli-Q water for 48 h in semipermeable membrane of 1000 Da molecular weight cutoff.

In Vitro Drug Release Kinetics

Since the synthesized nanoparticles possess a polyester backbone, they are susceptible to enzymatic hydrolysis under physiological conditions. The release kinetics of doxorubicin (DOX) from these nanoparticles was investigated through an *in vitro* degradation study conducted using enzyme esterase. The experiment was carried out at 37 °C with the buffer system maintained at a physiological pH of 7.4. The DOX-loaded polymeric nanoparticles were suspended in 1× PBS, and 10 units of esterase were added. This suspension was then placed into a 1000 Da molecular weight cutoff dialysis bag and dialyzed against 2 mL of 1× PBS. For the control, a similar setup was used, but esterase was not added to the nanoparticle suspension. Samples from the external dialysis medium were collected at predetermined time intervals and analyzed for DOX concentration using UV−vis spectroscopy.

Cell Viability Assay (MTT Assay)

The polymer nanoparticles were sterilized by exposure to UV light under a laminar-airflow chamber for 1 h prior to conducting biological

https://doi.org/10.1021/acspolymersau.4c00013
ACS Polym. Au 2024, 4, 392−404

studies. The biocompatibility of the polymer alone, free DOX, and P_{ST}-DOX was evaluated using the MTT assay in human breast cancer cell lines (MCF-7) following our earlier report.[36,37] Polymer nanoparticle samples, with or without a drug or dye, were dissolved in complete media and added to each well. The cells were incubated for 72 h in an atmosphere of 5% CO_2 and 1% O_2. To study cell viability, a standard MTT assay was typically carried out by starting with 1000 cells per well in a 96-well plate. However, the cells will proliferate over time with incubation, and they grow to more than 10,000 cells at the end of the MTT assay at 72 h. Control experiments were also performed in triplicate, where cells were seeded without any cargo or polymer. Following this incubation period, the medium was aspirated, and an MTT solution (0.5 mg/mL) in complete media was added. The plates were incubated for another 4 h to allow mitochondrial reductase in live cells to convert MTT to formazan. After 4 h, the medium was removed, and 100 μL of HPLC-grade dimethyl sulfoxide (DMSO) was added to each well to dissolve the formazan crystals, resulting in a purple-colored solution. Absorbance at 570 nm was recorded using a Varioskan microplate reader. Cell viability was determined based on the formazan concentration and compared to control values. All experiments were conducted in triplicate.

Cellular Uptake Studies for Drug- or Dye-Loaded Polymeric Nanoparticles

The uptake of drug- or dye-loaded polymeric nanoparticles was evaluated by fixed-cell imaging techniques. MCF-7 breast cancer cells were selected for these experiments. Cells were cultured on sterilized coverslips placed in a 6-well plate, with each well receiving 10^5 cells and 2.0 mL of complete media. The cells were incubated at 37 °C in an atmosphere of 5% CO_2 and 1% O_2 for 16 h. The polymeric nanoparticles were prepared by reconstituting the lyophilized polymer in complete media, and this solution was added to the wells containing the cells. The plate was then incubated for an additional 4 h under the same conditions. Following incubation, the cells were fixed to microscopic slides using the following protocol: the medium was aspirated, and the cells were washed twice with 1× PBS. A 4% paraformaldehyde solution was then added to the wells, and the cells were incubated at 4 °C for 20 min to achieve fixation. After fixation, the cells were washed twice with 1× PBS. Subsequently, the cells were stained with DAPI solution for 1 min to visualize the nuclei followed by washing off excess DAPI with 1× PBS. To prepare the slides for imaging, a 70% glycerol solution was added, and coverslips were secured using nail polish to ensure proper sealing and exposure to the glycerol solution. The prepared slides were left to air-dry for 12−18 h before imaging. Imaging was performed using a Leica SP8 confocal microscope, and image analysis was conducted using ImageJ software.

Flow Cytometry Experiments for Cellular Uptake of Free DOX and P_{ST}-DOX

The intracellular uptake of free doxorubicin (DOX) and DOX-encapsulated random copolymer nanoparticles was quantitatively assessed in MCF-7 breast cancer cells utilizing flow cytometry. MCF-7 cells were cultured in a 6-well plate at an initial density of 10^5 cells per well in complete media followed by an incubation period of 16 h at 37 °C under standard physiological conditions. Postincubation, cells were exposed to a 5 μg/mL concentration of either free DOX or DOX-loaded nanoparticles for 4 h. Subsequently, the medium containing the drug was aspirated, and the cells were washed with 1 mL of PBS. To detach the cells, 500 μL of trypsin was added followed by a 1 min incubation. The cell suspension was then subjected to centrifugation at 1000 rpm for 5 min. The resultant cell pellet was resuspended in 1 mL of PBS for flow cytometric analysis. Flow cytometry was conducted using a BD LSRFortessa SORP cell analyzer, which is equipped with five lasers and capable of detecting 18 distinct fluorescence channels simultaneously. Excitation of DOX was achieved with a 561 nm laser, and emission was detected using a band-pass filter cantered at 610 ± 10 nm.

RESULTS AND DISCUSSION

The L-aspartic acid consists of two carboxylic acid groups, which were converted to dimethyl esters under acidic conditions. The amine group of resultant compound **1** ((*S*)-1,4-dimethoxy-1,4-dioxobutan-2-aminium chloride) was modified as an amide for the synthesis of two different monomers, namely, M-AC and M-ST, as shown in Scheme 1. In the monomers, M-AC and M-ST were composed of acetal and stearate groups, respectively, as the side-chain pendant. In the case of the synthesis of the M-ST monomer, the amine group of compound **1** was coupled with stearic acid using an acid chloride coupling reaction.[37] Meanwhile, for the synthesis of the M-AC monomer, compound **2** (2,2,5-trimethyl-1,3-dioxane-5-carboxylic acid) was prepared by the reaction between 2,2-dimethoxy propane with bis(hydroxyl methyl) propionic acid under acidic conditions. The compound **1** was coupled to 2,2,5-trimethyl-1,3-dioxane-5-carboxylic acid (compound 2) using EDC coupling to produce M-AC.[36] The syntheses of the monomers are shown in Scheme 1. The structures of monomers and the intermediate compound were characterized by NMR, and their ^{1}H and ^{13}C spectra are provided as Figures S1−S6. Both of the monomers were subjected to thermogravimetric analysis, and they were found to be stable up to 180 °C, which is found to be suitable for melt condensation polymerization. TGA of the monomers further shows that M-ST is more thermally stable as compared to M-Ac as shown in Figure S7. The polyesters were synthesized by employing a solvent-free melt polycondensation approach by taking the dimethyl ester monomer of aspartic acid along with the 1,12-dodecane diol monomer (see Scheme 1). For the synthesis of P-ST (homopolymer of the stearate units), monomer M-ST and 1,12-dodecane diol were added in the test tube-shaped polymerization tube along with a Ti catalyst. The polymer reaction mixture was then subjected to polycondensation in two steps: (i) in the first step, M-ST and 1,12-dodecane diol were melted at 140 °C to produce oligomers of 2−6 repeating units, and (ii) in the second step, a high vacuum of 0.01 mbar was applied at 140 °C to accomplish more than 98% conversion in the melt process.

The structure of polymer P-ST was confirmed by ^{1}H NMR spectroscopy. During the melt transesterification polycondensation, the six protons corresponding to the two methoxy (−$COOCH_3$) groups in the M-ST monomer at 3.68 and 3.78 ppm vanished, and a new ester backbone (−CH_2OOC−) appeared at 4.07 and 4.15 ppm. The number of repeating units (degree of polymerization, X_n) was determined by comparing the intensity of end groups at 3.68 and 3.78 ppm with new ester groups at 4.07 and 4.14 ppm. The degree of polymerization X_n was found to be more than 97%. The ^{1}H and ^{13}C spectra of the P-ST polymer are shown in Figures S8 and S9. Following the similar polymerization procedure, the polymer P-AC was synthesized and characterized with NMR spectroscopy in Figures S10 and S11. A similar polymerization methodology was adopted for the synthesis of copolymers as employed for the homopolymer except that the molar ratio of the dimethyl ester monomers was varied with respect to 1,12-dodecane diol. For example, the copolymer PST_{10} stands for the polymer with 10% M-ST units and 90% M-Ac units in the polymer backbone. To synthesize the PST_{10} copolymer, the 1,12-dodecane diol percentage of the molar ratio was kept fixed as 100%, and with respect to it, M-ST was taken as 10% and the remaining 90% was maintained using M-Ac. In this way,

https://doi.org/10.1021/acspolymersau.4c00013
ACS Polym. Au 2024, 4, 392−404

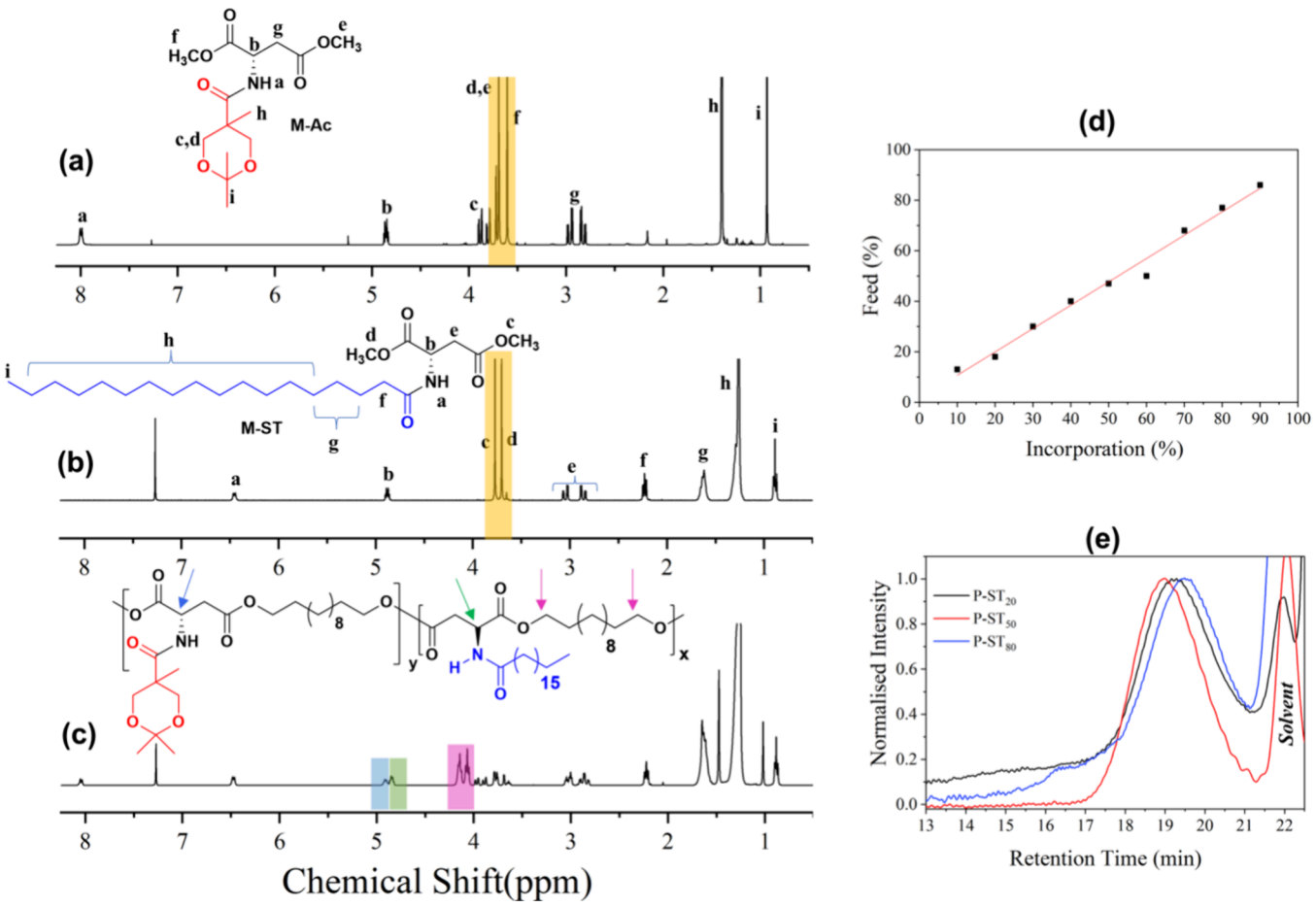

Figure 2. ^{1}H NMR spectra of the (a) M-Ac, (b) M-ST, and (c) P-ST$_X$ copolymer (different peaks in the monomers are assigned alphabetically). (d) Plot of feed versus incorporation of stearic units in the copolymer determined by ^{1}H NMR. (e) SEC chromatograms of P-ST$_X$ copolymers recorded in THF as an eluent at 25 °C.

the ratio of dimethyl ester and diol monomers was kept at 1:1, and polymerization was performed. The synthesized copolymers were characterized by NMR spectroscopy as shown in Figure 2. To study the monomer incorporated in the P-ST$_X$ copolymer, the ^{1}H NMR spectra of the copolymer are compared with the monomers M-Ac and M-ST. By comparing the monomer and copolymer ^{1}H NMR spectra (Figure 2a–c), it can be concluded that during the polymerization, the side-chain pendants such as acetal and stearate groups remain intact and do not interfere in the polymerization. The methyl ester peak belonging to the monomers gets consumed to produce a new ester backbone appearing at 4.12 and 4.02 ppm (highlighted in pink color). Following the similar procedure, a series of copolymers with different compositions were synthesized and characterized such as PST$_{20}$, PST$_{30}$, and PST$_{40}$ until PST$_{90}$ depending upon % of M-ST units incorporated in the copolymer chain. The peak highlighted in a blue color belongs to the acetal unit, while the green peak corresponds to the stearate unit; upon comparison of the integration ratio of these two monomers, the percentage incorporation of the acetal and stearate units in the polymer chain was determined. Similarly, all of the copolymers were characterized. ^{1}H NMR spectra of other copolymers are provided as Figures S12–S20. The percentage incorporation of the stearic segments in the polymer was calculated from the ^{1}H NMR spectrum of the copolymer shown in Figure 2d. The plot of feed vs incorporation for the acetal unit is shown in Figure 2d. The feed vs incorporation plot shows a linear trend, which suggests the good reproducibility of the copolyester synthesis. The synthesized polymer was further studied for the molecular weight using size exclusion chromatography (SEC) with tetrahydrofuran (THF) as an eluent and calibrated with a polystyrene standard. The SEC chromatogram for a few copolymers is shown in Figure 2e. The polymer produced a moderate to higher molecular weight with monomodal distribution (the SEC chromatogram for other polymers is provided as Figure S21). The molecular weight of polymers obtained in the case of P-ST$_X$ random copolymers was moderate to high, with M_n ranging from 7.4 × 10^3 to 16.5 × 10^3 g/mol. Meanwhile, the weight-average molecular weight (M_w) ranges from 15.0 × 10^3 to 25.4 × 10^3 g/mol with a polydispersity index close to 2.0, which was expected for the melt polycondensation. The molecular weights obtained are summarized in Table 1. The acetal pendant group from the P-ST$_X$ random copolymer was deprotected with trifluoracetic acid (TFA) to produce hydroxyl polymer stearate pendants as shown in Scheme 2. The deprotected polymer was characterized by ^{1}H NMR (see Figure S22). The polymer P-ST$_X$ peak at 1.47 ppm corresponding to acetal vanished after deprotection, while other backbone peaks remain intact, which confirms the successful deprotection of the P-ST$_X$ polymer, in which stearate units remain intact during deprotection. The deprotected polymer is denoted as PST$_X$-OH, which corresponds to the deprotected version of P-ST$_X$ polymers.

https://doi.org/10.1021/acspolymersau.4c00013
ACS Polym. Au 2024, 4, 392–404

Table 1. Table Showing Feed vs Incorporation in the Polymer and SEC Molecular Weights

	feed[a] (%)		incorporated[b] (%)				
polymer	M-Ac	M-ST	acetal	stearic	M_n[c] (g/mol)	M_w[c] (g/mol)	Đ[c]
P-AC	100	0	100	0	11,700	20,400	1.7
P-ST$_{10}$	90	10	86	14	14,000	18,000	1.3
P-ST$_{20}$	80	20	77	23	16,500	25,700	1.5
P-ST$_{30}$	70	30	68	32	7600	14,800	1.9
P-ST$_{40}$	60	40	59	41	14,400	25,600	1.7
P-ST$_{50}$	50	50	47	53	13,600	24,500	1.8
P-ST$_{60}$	40	60	40	60	13,000	23,800	1.8
P-ST$_{70}$	30	70	30	70	8800	17,000	1.9
P-ST$_{80}$	20	80	18	82	9000	15,400	1.7
P-ST$_{90}$	10	90	13	86	7400	15,000	2.0
P-ST	0	100	0	100	8500	15,000	1.7

[a]Percentage of the monomers in the feed. [b]Percentage of the units incorporated in the polymer backbone determined by ^{1}H NMR. [c]The number-average molecular weight (M_n), weight-average molecular weight (M_w), and dispersity were determined by SEC using THF as an eluent at 25 °C.

Scheme 2. Synthesis of Hydroxyl-Functionalized Random Copolymers

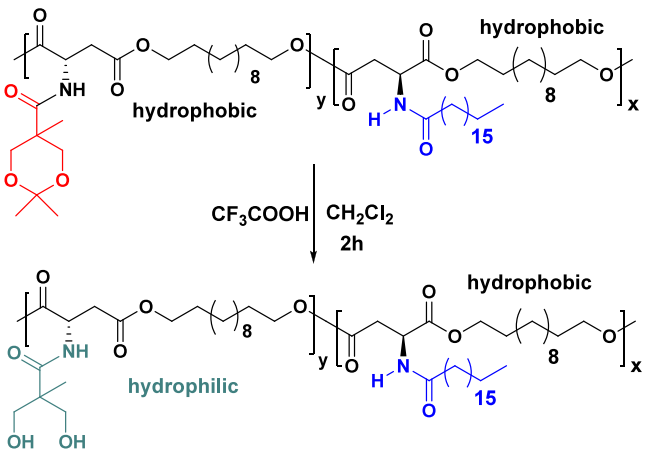

The polyesters were subjected to thermogravimetric analysis (TGA) and differential scanning calorimetry (DSC) to study their thermal properties. TGA data reveal that polymers are stable up to 280 to 300 °C (see Figure 3a). Differential scanning calorimetry studies showed that the polymer P-Ac is amorphous in nature as shown in Figure 3b with a glass transition (T_g) temperature of −20 °C, while P-ST (stearate-substituted polymer) is found to be semicrystalline with a melting point of 42 °C as shown in Figure 3c. As the copolymer is prepared by mixing these two different monomers that are acetal and stearate, the copolymer becomes semicrystalline (see Figure 3d). This semicrystalline nature of the polymer is attributed to the presence of the stearate side chain in the polymer backbone, which produces a crystalline domain in the polymer matrix. The van der Waals interaction between the stearate pendant in the polymer causes formation of the nucleating site for the formation of the crystalline domain. It was clearly observed that an increase in percentage of the stearate unit in the polymer increases the rigidity in packing of the polymer chain, which is reflected in terms of the melting point of the polymer. The polymers were also studied for thermal stability after deprotection, as shown in Figure S23, and the polymers showed a much lower decomposition temperature as compared to the acetal counterpart; this reduction in stability is due to the presence of a free hydroxyl group in the side chain of the polymer, which causes backbiting on the polyester backbone. The nature of PST$_X$-OH polymers was further compared to P-ST$_X$ polymers, and Figure 3e shows the DSC thermogram for PST$_{20}$-OH. The DSC thermograms for all the P-ST$_X$ and PST$_X$-OH polymers are shown in Figures S24−S27. After the deprotection of the acetal group, the polymer shows a small difference in the thermal properties, and both the melting point and crystallization temperature increase with the stearate content in the polymer backbone, as shown in Figure 3f.

The P-ST$_X$ polymers are hydrophobic in nature and do not show solubility in water as they are composed of acetal and stearate side chains, while the polymer attains hydrophilicity after deprotection of the acetal group pendant to the hydroxyl group in the polymer. The PST$_X$-OH polymer is composed of both hydrophobic and hydrophilic units; the hydroxy group serves as a hydrophilic segment, while the long-chain stearate group serves as a hydrophobic group in the polymer. The polymer attains enough amphiphilic balance to form stable nanoparticles in water. Polymers with different contents of hydroxyl and stearate were attempted for self-assembly in the water by a dialysis method. In the dialysis method of nanoparticle synthesis, 5.0 mg of the polymer was dissolved 2.0 mL of dimethyl sulfoxide and was added with 3.0 mL of deionized water dropwise. The solution was then transferred to a dialysis tube of 1000 Da MWCO and dialyzed against deionized water for 48 h; water was replenished in a reservoir after regular intervals of time. All PST$_X$-OH polymers with different compositions of stearate pendant and hydroxyl groups were attempted to make polymer nanoparticles using the dialysis method. Among the different PST$_X$-OH copolymers, the polymer with up to 50% stearate and hydroxyl pendants was found to be producing nanoparticles, while polymers with more than 50% stearate units were unable to form stable nanoparticles and precipitate out after or during dialysis. The different hydroxyl-functionalized copolymer nanoparticles were characterized for their size, and it was found that NPs showed a size in the range of 500 nm, while the polymer PST$_{20}$-OH showed formation of stable polymer nanoparticles. Taking this into account, the polymer PST$_{20}$-OH was attempted to encapsulate various drugs and biomarkers in the polymer nanoparticles. The encapsulation of a drug or dye (biomarker) was carried out by the following procedure as mentioned for self-assembly; the only difference was the addition of a drug or biomarker along with the polymer during dialysis. The PST$_{20}$-OH polymer (5.0 mg) was dissolved along with 0.5 mg of the drug or biomarker in 2 mL of HPLC-grade DMSO. This solution was then added with deionized water slowly dropwise with continuous stirring to avoid early precipitation of the polymer. After complete addition of the polymer, the resulting solution was then transferred in a semipermeable membrane of MWCO 1000 Da and dialyzed for 48 h against deionized water. The primary concept of this project is the development of amphiphilic nanocarriers for drug or biomarker encapsulation. To demonstrate the proof of concept, various biomarkers and drugs were selected and loaded into the core of the polymeric micelles as the polymer nanoparticles attained sufficient amphiphilicity to form stable nanoparticles. Various drugs and biomarkers were attempted to encapsulate inside the

https://doi.org/10.1021/acspolymersau.4c00013
ACS Polym. Au 2024, 4, 392−404

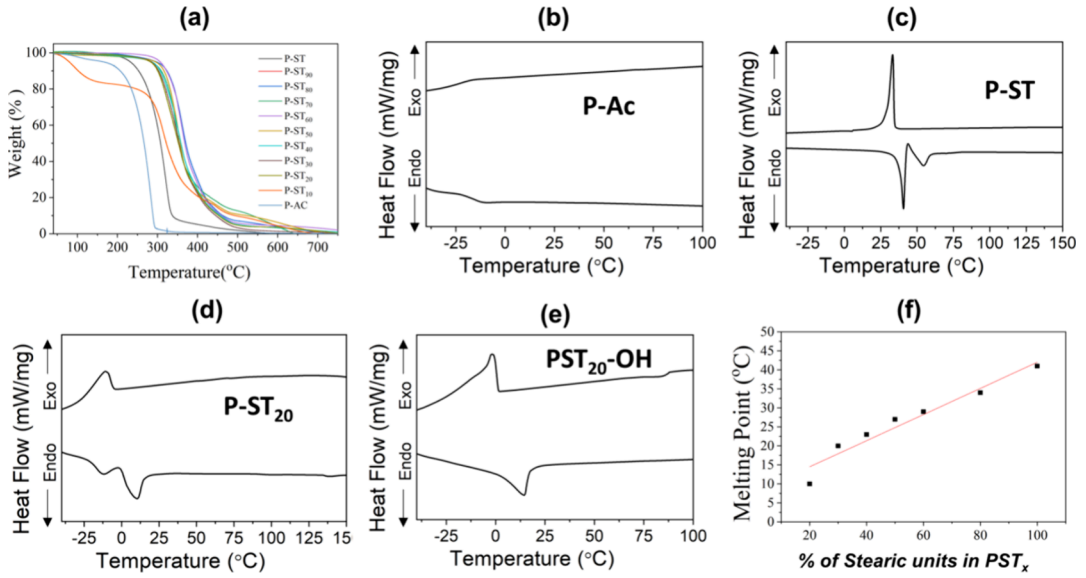

Figure 3. (a) TGA thermograms of homo and all copolymers. TGA was recorded from 40 to 800 °C under a nitrogen atmosphere. DSC profiles of (b) P-Ac, (c) P-ST, (d) P-ST_{20}, and (e) PST_{20}-OH. (f) Plot % of M-ST in the P-ST_X polymer vs melting point of the polymers determined from the DSC thermogram.

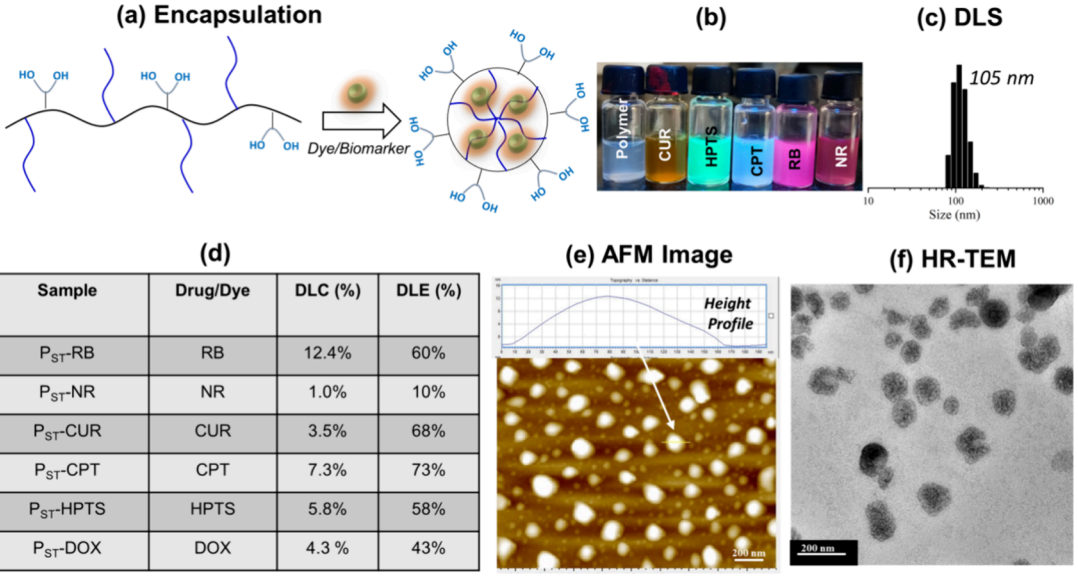

Sample	Drug/Dye	DLC (%)	DLE (%)
P_{ST}-RB	RB	12.4%	60%
P_{ST}-NR	NR	1.0%	10%
P_{ST}-CUR	CUR	3.5%	68%
P_{ST}-CPT	CPT	7.3%	73%
P_{ST}-HPTS	HPTS	5.8%	58%
P_{ST}-DOX	DOX	4.3 %	43%

Figure 4. (a) Diagrammatic illustration of drug/dye encapsulation in PST_{20}-OH water-based self-assembly. (b) Picture of drug and dye-loaded nanoparticles taken in UV light. (c) DLS histogram for polymeric self-assembly loaded with a drug. (d) Table containing the DLC and DLE values. (e) AFM image and (f) HR-TEM image of P_{ST}-DOX nanoparticles at 0.1 mg/mL (scale bar for AFM and HR-TEM = 200 nm).

nanocavity of the nanoparticles; among them, the following biomarkers such as Nile red (NR), rose bengal (RB), and 8-hydroxypyrene-1,3,6-trisulfonic acid (HPTS) and drugs such as doxorubicin (DOX), curcumin (CUR), and camptothecin (CPT) were encapsulated inside the nanoparticles (the chemical structure of the cargo shown as Figure S28).

The amphiphilicity of the polymer is controlled by the ratio of the hydroxyl to stearate units. The interaction of the hydroxyl functional groups in the polymer backbone with the drug or biomarkers occurs during loading during the dialysis process. It was found that a higher content of stearate units in the polymer led to the destabilization of nanoparticles, resulting in the precipitation of polymer nanoparticles. Phase segregation of the hydroxyl group occurs during encapsulation, which assists in the loading of cargos into the core of the polymer nanoparticles. The schematic representation of loading of drugs/dyes inside the nanocavity is shown in Figure 4a. The polymer PST_{20}-OH present in the extended confirmation in the DMSO, during dialysis, undergoes phase segregation as the content of water increases in the dialysis medium, resulting in the formation of polymeric nanoparticles. These polymer nanoparticles have a hydrophobic cavity at the core, which is made from the stearate unit, and it is able to encapsulate various hydrophobic cargos, while the corona was occupied by hydroxyl pendants of the polymer. The drug- or biomarker-loaded nanoparticles were denoted as P_{ST}-HPTS for HPTS-loaded NPs; similarly, others are referred accordingly depending upon the loaded cargo. When UV light was irradiated on the polymer NPs encapsulating cargos, they showed bright-colored emission depending upon the loaded

https://doi.org/10.1021/acspolymersau.4c00013
ACS Polym. Au 2024, 4, 392−404

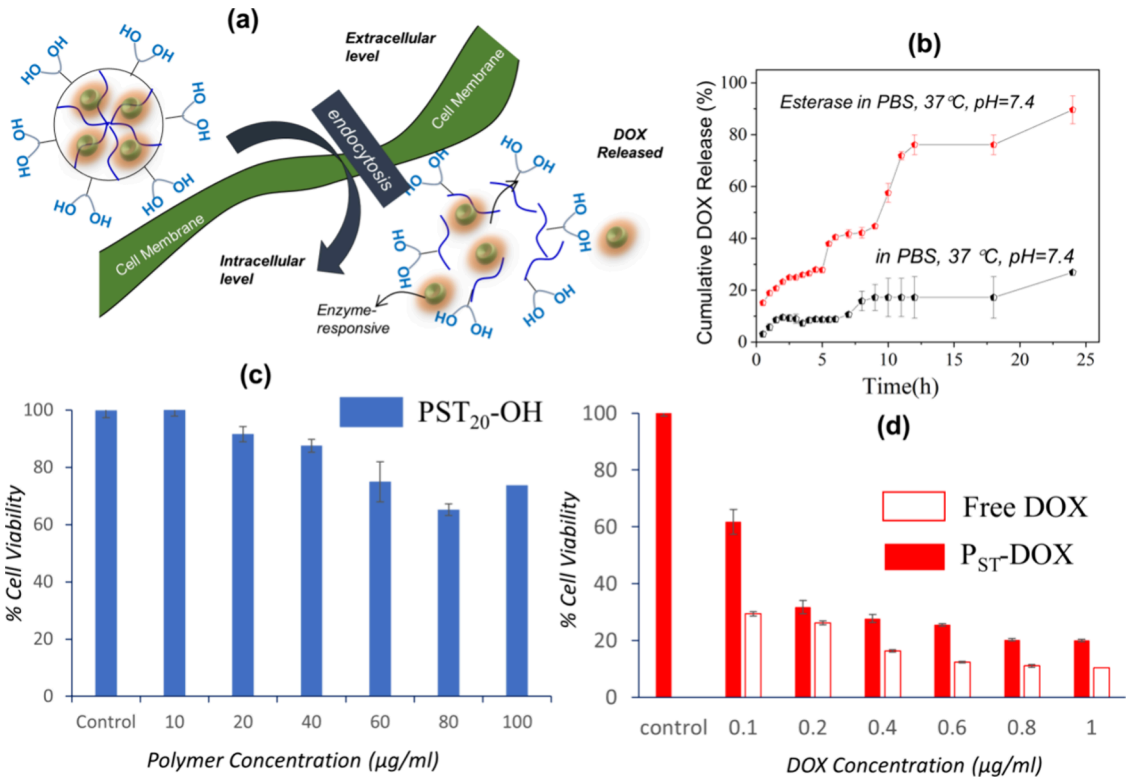

Figure 5. (a) Enzymatic biodegradation of polymer nanoparticles in the lysosomal compartment of the cells after the endocytosis of P_{ST}-DOX by MCF-7 cell lines. (b) Cumulative profile of doxorubicin release from P_{ST}-DOX nanoparticles. (c) Cell viability of the PST_{20}-OH polymer in the MCF-7 cell lines. (d) Cell viability of P_{ST}-DOX and free DOX. In the cytotoxicity assays, 10^3 cells are employed as seeding. The experiments were performed in triplicates, $N = 3$.

cargo (see Figure 4b). The polymer NPs were then characterized for the size using DLS; P_{ST}-CPT was found to produce polymer NPs of 105 ± 10 nm as shown in Figure 4c. DLS was carried out for other drug-/dye-loaded polymer NPs; results further suggest formation of nanoparticles of ≤250 nm with a PDI less than 0.5, with the data for others provided as Figure S29. The self-assembled polymers were then characterized by absorbance for calculating the drug/dye loading content (DLC) and drug/dye loading efficacy (DLE) using Lambert−Beer's law using the equation provided in the Experimental Section. Among the different loaded cargos, RB showed the highest 12% DLC with 60% DLE, while NR showed the lowest DLC of about 1% and 10% DLE. The table in Figure 4d summarizes DLC and DLE of various cargos loaded in polymer NPs. The P_{ST}-DOX was characterized for its shape and size using AFM and HR-TEM. The AFM image shows the formation of spherical polymer nanoparticles with a size less than 250 nm, which can be seen from the height profile provided in Figure 4e. The HR-TEM image for the P_{ST}-DOX is shown in Figure 4f, which further confirms the spherical shape and size of the polymer nanoparticles of less than 250 nm. Absorbance and emission plots for the polymer NPs suggest that there is no difference in the photophysical properties of the cargo after being loaded inside the hydrophobic core of nanoparticles as shown in Figure S30. The stability of the nanoparticles in water, 10% PBS, and 10% FBS was assessed using DLS over the course of a week, and it was found that the polymer nanoparticles remained stable under all tested conditions, as shown in Figure S31. It is very well-known that lysosomal enzymes found in intracellular compartments biodegrade aliphatic polyester polymeric nanoparticles, causing release of encapsulated cargos as seen in Figure 5a. The polymeric nanoparticles taken up by the cells by the process of endocytosis go through the early endosome, late endosome, and finally to the lysosome. The lysosome is an enzyme-rich compartment of the cells having hydrolytic or degrading enzymes such as protease, esterase, chymotrypsin, etc., which acts on the polymer nanoparticle causing it to cleave the aliphatic ester backbone, ultimately releasing the loaded cargo. An *in vitro* experiment was designed to investigate the enzyme stimulus-responsive drug releasing properties of the P_{ST}-DOX polymer NPs. A 1000 Da dialysis tube was filled with the polymeric solution containing the horse liver esterase enzyme. The P_{ST}-DOX sample was incubated at 37 °C, the physiological temperature, with 10 U of the horse liver esterase enzyme in PBS at pH = 7.4. The outside reservoir was filled with PBS of pH 7.4, the samples were collected, and absorbance was recorded, which enabled monitoring of the discharged doxorubicin.

Doxorubicin release kinetics was also investigated as a control experiment in PBS alone at pH 7.4 in the absence of an enzyme. The DOX release was tracked by absorbance spectroscopy. Nearly up to 90% DOX was released from polymer nanoparticles, when an enzyme was present in the dialysis bag, as shown by the plot in Figure 5b. Upon incubation of the polymer nanoparticles with PBS, a partial destabilization of the nanoparticles occurred in the early stage, leading to leaching of loaded cargos. Subsequent destabilization and release occurred due to the action of enzymes on the polymer nanoparticles. The influence of PBS salt and swelling of nanoparticles account for the partial destabilization of the NPs at 37 °C and are responsible for the 20% drug leaching

https://doi.org/10.1021/acspolymersau.4c00013
ACS Polym. Au 2024, 4, 392−404

out. A degradation study for the random copolyester PST_{20}-OH was conducted using size exclusion chromatography (SEC) as shown in Figure S32. The polymer's molecular weight decreases with respect to the degradation in the presence of an enzyme. It is critical to comprehend the biocompatibility of any polymeric biomaterial with various cell types under physiological conditions. The cytotoxicity of the PST_{20}-OH polymer nanoparticles and DOX (anticancer drug)-loaded polymer nanoparticles (P_{ST}-DOX) was investigated using the MTT assay. To study cell viability of PST_{20}-OH polymer nanoparticles, the concentration of the polymer was examined between 10 and 100 μg/mL. Cell viability data for MCF-7 cell lines are shown as seen in Figure 5c. The breast cancer cell lines MCF-7 and the normal cell line wild-type mouse embryonic fibroblast (WT MEF) were selected for the cytotoxicity study (see Figure S33). The polymer PST_{10}-OH was found to be biocompatible up to the concentration of 100 μg/mL; it was revealed that both malignant cell lines as well as normal cell lines remain unaffected by the polymer PST_{10}-OH (see Figure 5c and Figure S33 for WT-MEFs). The cytotoxicity of the P_{ST}-DOX and free DOX was examined similarly as performed for the polymer nanoparticles. The DOX concentration was kept within a range of 0.1 to 1.0 μg/mL, and an MTT assay was performed for both normal and cancerous cell lines. In Figure 5d, cell viability data in MCF-7 cell lines for P_{ST}-DOX are shown as a histogram, which shows that P_{ST}-DOX polymer NPs are effective in inhibiting the cancer cell growth as compared to the free DOX. FACS analyses were carried out to study the ability of the nanoparticles to undergo cellular uptake by the cells. It was found that the polymer nanoparticle was taken up by the cells in a higher concentration as compared to the free DOX as shown in Figure S34. The PST_{20}-OH polymer nanoparticles' capacity to undergo endocytosis and deliver the various loaded cargos across the cell membrane was investigated by using the MCF-7 cell line. The cellular uptake of polymer nanoparticles by the MCF-7 cell lines was studied using confocal laser scanning microscopy (CSLM). The cells were grown on glass coverslips in a 6-well plate in complete media for 18 h. Subsequently, after 18 h, when cells get adhered on the surface of the coverslip, the medium from the well was aspirated and fresh complete media with drug- or biomarker-loaded polymer NPs were added and plate incubated for 4 h. The concentration of the drug or biomarker was maintained as 5 μg for each chromophore. The cells were stained with a nucleus staining dye such as DAPI and acridine orange (AO) depending upon uptake of loaded cargos. While staining the nuclease of the cells with different dyes, it was taken care that the excitation source of nuclear stain should not overlap with cargos inside the polymer nanoparticles; for example, while studying the cellular uptake of P_{ST}-DOX, P_{ST}-RB, and P_{ST}-NR, the nucleus of the cells was stained using DAPI. While AO stain was used for uptake of P_{ST}-HPTS, P_{ST}-CUR, and P_{ST}-CPT polymer nanoparticles. Different biomarkers and drugs were utilized for cellular uptake studies, necessitating the use of specific nuclear dyes. DAPI was used for DOX, RB, and NR cargos as it does not interfere with bioimaging of these cell lines. Conversely, acridine orange was used for CPT, CUR, and HPTS uptake studies because DAPI can interfere with the bioimaging of these chromophores, which require excitation with a 405 nm laser. This selection ensures accurate imaging results for each respective drug. CSLM images of the P_{ST}-DOX, P_{ST}-RB, and P_{ST}-HPTS are shown in Figure 6, while cellular uptake images of other cargos such as P_{ST}-NR, P_{ST}-CUR, and P_{ST}-CPT are provided as Figure S35.

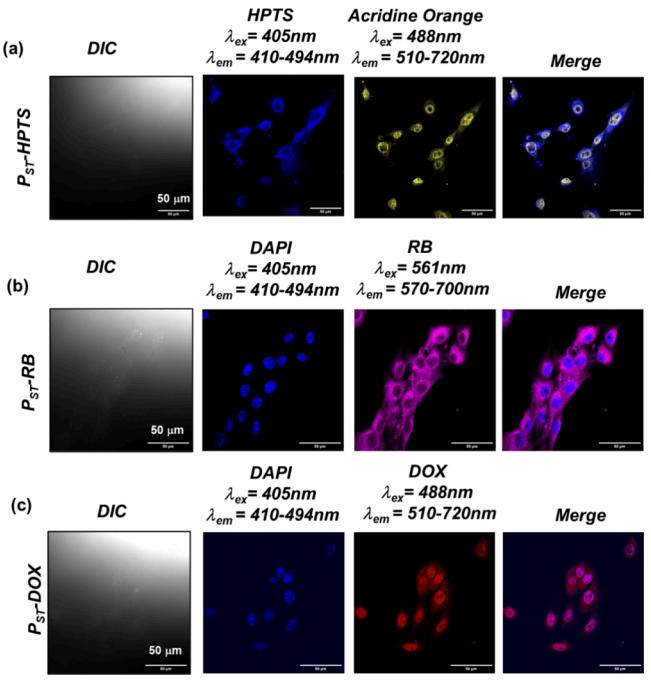

Figure 6. Confocal images of cellular uptake of (a) P_{ST}-HPTS, (b) P_{ST}-RB, and (c) P_{ST}-DOX in the MCF-7 cell line [4 h of incubation; 10^5 cells were seeded]. Concentrations of the RB, DOX, and HPTS were maintained as 5.0 μg/mL. Scale bar = 50 μm.

The first panel in Figure 6a shows the cellular uptake studies of P_{ST}-HPTS for a 4 h time point, while imaging HPTS in the cells was excited with a 405 nm laser in a confocal laser scanning microscope, and for collection of emission signal in the range of 410 to 494 nm, the signal was given a pseudo blue color, which confirms uptake of P_{ST}-HPTS; in this case, acridine orange (AO) nuclear stain was excited at 488 nm, and collection was done between 510 and 570 nm. HPTS signals were observed from the cytoplasm of the cells. Similarly, another biomarker-encapsulated polymer NP P_{ST}-RB uptake study is shown in Figure 6b; in this case, DAPI was used as a nuclear stain; the cells show signal from the cytoplasm of the cells, which can be confirmed from the merged image. P_{ST}-DOX uptake is shown in Figure 6c, similar to the rose bengal nucleus stained with DAPI. DOX and RB were excited at 488 and 561 nm, respectively; collection of signals was done at 510−720 nm for DOX, while for RB, it was collected at 570−700 nm. The signal from DOX is shown as a pseudo red color, while from RB is shown in the pink color. At a 4 h time point, the signal of loaded cargos was found to be coming from the cytoplasm of the cells. The cellular uptake images of P_{ST}-NR, P_{ST}-CUR, and P_{ST}-CPT are provided as Figure S35. In CSLM, the cargos were excited using different lasers depending upon their excitation spectra. This study confirms that the polymer PST_{20}-OH is capable to encapsulate the biomarker and drug, which is further used for delivery in side the cells and effective inhibition of the cell growth upon delivery of DOX using polymer nanoparticles.

https://doi.org/10.1021/acspolymersau.4c00013
ACS Polym. Au 2024, 4, 392−404

CONCLUSIONS

L-Aspartic acid-based P-ST$_X$ random copolymers were synthesized using a solvent-free melt polycondensation strategy with a perfect feed vs incorporation ratio. The control of acetal to stearate units in the polymer was maintained at the stage of polymerization by carefully maintaining the feed ratio of the monomers. These copolymers were characterized with the help of NMR spectroscopy, size exclusion chromatography, etc., which suggests the formation moderate- to high-molecular-weight polymers with monomodal distribution. The acetal-functionalized polymers were found to be hydrophobic in nature, while it was converted into the hydrophilic hydroxyl-functionalized group by selective deprotection of the acetal pendant groups under acidic conditions. The polymers were characterized for thermal properties using TGA and DSC. These polymers were found to be thermally stable up to 280 to 300 °C. DSC data of the polymer further suggest that the acetal-functionalized polymer is amorphous in nature, while after incorporation, the stearate unit in the polymer induces a semicrystalline nature. A further increase in the content of stearate units increases the melting point of the copolymers. The hydroxyl-functionalized copolymers were found to be dispersible in water and formed stable nanoparticles in water, which were capable of loading various cargos. Due to the presence of the polyester backbone in the polymer, it shows enzyme-responsive release of loaded cargos. Further cytotoxicity studies carried out for polymer NPs suggest that polymers and polymers loaded with a biomarker are nontoxic toward normal and cancer cell lines. Meanwhile, polymers loaded with DOX showed growth inhibition of the cancer cells, which suggest that polymer NPs showed good drug delivery capabilities. The cellular uptake in MCF-7 cell lines was carried out, which confirms the uptake of NPs inside the cells.

ASSOCIATED CONTENT

Supporting Information

The Supporting Information is available free of charge at https://pubs.acs.org/doi/10.1021/acspolymersau.4c00013.

Synthesis of polymers, NMR spectra of monomers and polymers, TGA of monomers and polymers, DSC thermograms of polymers, DLS data of the drug and dye-loaded polymer nanoparticles, absorbance and emission spectra, SEC plots, MTT assay, confocal microscope images, and FACS data (PDF)

AUTHOR INFORMATION

Corresponding Author

Manickam Jayakannan − *Department of Chemistry, Indian Institute of Science Education and Research (IISER Pune), Pune, Maharashtra 411008, India;* orcid.org/0000-0001-7699-2016; Email: jayakannan@iiserpune.ac.in

Authors

Mohammed Khuddus − *Department of Chemistry, Indian Institute of Science Education and Research (IISER Pune), Pune, Maharashtra 411008, India*

Utreshwar Arjun Gavhane − *Department of Chemistry, Indian Institute of Science Education and Research (IISER Pune), Pune, Maharashtra 411008, India*

Complete contact information is available at: https://pubs.acs.org/10.1021/acspolymersau.4c00013

Author Contributions

The manuscript was written through contributions of all authors. All authors have given approval to the final version of the manuscript. CRediT: **Mohammed Khuddus** data curation, formal analysis, investigation, methodology, validation, visualization, writing-original draft, writing-review & editing; **Utreshwar Arjun Gavhane** data curation, formal analysis, investigation, methodology, validation, visualization, writing-original draft, writing-review & editing; **Manickam Jayakannan** conceptualization, formal analysis, funding acquisition, investigation, project administration, resources, supervision, validation, writing-original draft, writing-review & editing.

Notes

The authors declare no competing financial interest.

ACKNOWLEDGMENTS

M.K. and U.A.G. thank UGC India for the PhD fellowship. The authors acknowledge the research grant (project code CRG/2019/000496) from the Science and Engineering Research Board (SERB), New Delhi, India. We thank the IISER Pune Microscopy Facility for cellular imaging and the PerkinElmer-IISER Pune, Centre of Excellence facility.

REFERENCES

(1) Tang, S.; Gao, Y.; Wang, W.; Wang, Y.; Liu, P.; Shou, Z.; Yang, R.; Jin, C.; Zan, X.; Wang, C.; Geng, W. Self-Report Amphiphilic Polymer-Based Drug Delivery System with ROS-Triggered Drug Release for Osteoarthritis Therapy. *ACS Macro Lett.* **2024**, *13* (1), 58−64.

(2) Pandey, B.; Patil, N. G.; Bhosle, G.; Ambade, A. V.; Gupta, S. S. Amphiphilic Glycopolypeptide Star COPOLYMER-Based Cross-Linked Nanocarriers for Targeted and Dual-Stimuli-Responsive Drug Delivery. *Bioconjugate Chem.* **2019**, *30*, 633−646.

(3) Patra, D.; Kumar, S.; Kumar, P.; Chakraborty, I.; Basheer, B.; Shunmugam, R. Iron(III) Coordinated Theranostic Polyprodrug with Sequential Receptor-Mitochondria Dual Targeting and T1-Weighted Magnetic Resonance Imaging Potency for Effective and Precise Chemotherapy. *Biomacromolecules* **2022**, *23* (8), 3198−3212.

(4) Yin, L.; Song, Z.; Kim, K. H.; Zheng, N.; Tang, H.; Lu, H.; Gabrielson, N.; Cheng, J. Reconfiguring the Architectures of Cationic Helical Polypeptides to Control Non-Viral Gene Delivery. *Biomaterials* **2013**, *34*, 2340−2349.

(5) Singh, S.; Paswan, K. K.; Kumar, A.; Gupta, V.; Sonker, M.; Khan, M. A.; Kumar, A.; Shreyash, N. Recent Advancements in Polyurethane-based Tissue Engineering. *ACS Appl. Bio Mater.* **2023**, *6*, 327−348.

(6) Liang, Y.; He, J.; Guo, B. Functional Hydrogels as Wound Dressing to Enhance Wound Healing. *ACS Nano* **2021**, *15*, 12687−12722.

(7) Exley, S. E.; Paslay, L. C.; Sahukhal, G. S.; Abel, B. A.; Brown, T. D.; McCormick, C. L.; Heinhorst, S.; Koul, V.; Choudhary, V.; Elasri, M. O.; Morgan, S. E. Antimicrobial Peptide Mimicking Primary Amine and Guanidine Containing Methacrylamide Copolymers Prepared by Raft Polymerization. *Biomacromolecules* **2015**, *16*, 3845−3852.

(8) Ghosh, R.; Jayakannan, M. Theranostic FRET Gate to Visualize and Quantify Bacterial Membrane Breaching. *Biomacromolecules* **2023**, *24*, 739.

(9) Yang, P. B.; Davidson, M. G.; Edler, K. J.; Brown, S. Synthesis, Properties, and Applications of Bio-Based Cyclic Aliphatic Polyesters. *Biomacromolecules* **2021**, *22*, 3649−3667.

(10) Jérôme, C.; Lecomte, P. Recent Advances in the Synthesis of Aliphatic Polyesters by Ring-Opening Polymerization. *Adv. Drug Delivery Rev.* **2008**, *60*, 1056−1076.

(11) Surnar, B.; Jayakannan, M. Stimuli-Responsive Poly-(caprolactone) Vesicles for Dual Delivery under the Gastrointestinal Tract. *Biomacromolecules* **2013**, *14*, 4377−4387.
(12) Buzin, P.; Lahcini, M.; Schwarz, G.; Kricheldorf, H. R. Aliphatic Polyesters by Bismuth Triflate-Catalyzed Polycondensations of Dicarboxylic Acids and Aliphatic Diols. *Macromolecules* **2008**, *41*, 8491−8495.
(13) Cai, Q.; Bai, T.; Zhang, H.; Yao, X.; Ling, J.; Zhu, W. Catalyst-Free Synthesis of Polyesters via Conventional Melt Polycondensation. *Mater. Today* **2021**, *51*, 155−164.
(14) Labet, M.; Thielemans, W. Synthesis of Polycaprolactone: A Review W. *Chem. Soc. Rev.* **2009**, *38*, 3484−3504.
(15) Woodruff, M. A.; Hutmacher, D. W. Progress in Polymer Science The Return of a Forgotten Polymer — Polycaprolactone in the 21st Century. *Prog. Polym. Sci.* **2010**, *35*, 1217−1256.
(16) Kamaly, N.; Yameen, B.; Wu, J.; Farokhzad, O. C. Degradable Controlled-Release Polymers and Polymeric Nanoparticles: Mechanisms of Controlling Drug Release. *Chem. Rev.* **2016**, *116*, 2602−2663.
(17) Middleton, J. C.; Tipton, A. J. Synthetic Biodegradable Polymers as Orthopedic Devices. *Biomaterials* **2000**, *21*, 2335−2346.
(18) Samadi, N.; Van Nostrum, C. F.; Vermonden, T.; Amidi, M.; Hennink, W. E. Mechanistic Studies on the Degradation and Protein Release Characteristics of Poly(Lactic-Co-Glycolic-Co-Hydroxymethylglycolic Acid) Nanospheres. *Biomacromolecules* **2013**, *14*, 1044−1053.
(19) Deming, T. J. Methodologies for Preparation of Synthetic Block Copolypeptides: Materials with Future Promise in Drug Delivery. *Adv. Drug Delivery Rev.* **2002**, *54*, 1145−1155.
(20) Deming, T. J. Synthesis of Side-Chain Modified Polypeptides. *Chem. Rev.* **2016**, *116*, 786−808.
(21) Carlsen, A.; Lecommandoux, S. Current Opinion in Colloid & Interface Science Self-Assembly of Polypeptide-Based Block Copolymer Amphiphiles. *Curr. Opin. Colloid Interface Sci.* **2009**, *14*, 329−339.
(22) Nisal, R.; Jayakannan, M. Tertiary-Butylbenzene Functionalization as a Strategy for β-Sheet Polypeptides. *Biomacromolecules* **2022**, *23*, 2667−2684.
(23) Kricheldorf, H. R. Polypeptides and 100 Years of Chemistry of a -Amino Acid N -Carboxyanhydrides Angew. *Chem. Int. Ed.* **2006**, *45*, 5752−5784.
(24) Ghaffar, A.; Draaisma, G. J. J.; Mihov, G.; Dias, A. A.; Schoenmakers, P. J.; Van der Wal, S. *Biomacromolecules* **2011**, *12*, 3243−3251.
(25) Deng, M.; Wu, J.; Reinhart-King, C. A.; Chu, C. C. Synthesis and Characterization of Biodegradable Poly(Ester Amide)s with Pendant Amine Functional Groups and in Vitro Cellular Response. *Biomacromolecules* **2009**, *10*, 3037−3047.
(26) Wu, J.; Wu, D.; Mutschler, M. A.; Chu, C. C. Cationic Hybrid Hydrogels from Amino-Acid-Based Poly(Ester Amide): Fabrication, Characterization, and Biological Properties. *Adv. Funct. Mater.* **2012**, *22*, 3815−3823.
(27) Fonseca, A. C.; Gil, M. H.; Simões, P. N. Biodegradable Poly(Ester Amide)s - A Remarkable Opportunity for the Biomedical Area: Review on the Synthesis, Characterization and Applications. *Prog. Polym. Sci.* **2014**, *39*, 1291−1311.
(28) Bourke, S. L.; Kohn, J. Polymers Derived from the Amino Acid L-Tyrosine: Polycarbonates, Polyarylates and Copolymers with Poly(Ethylene Glycol). *Adv. Drug Delivery Rev.* **2003**, *55*, 447−466.
(29) He, M.; Ro, L.; Liu, J.; Chu, C.-C. Folate-Decorated Arginine-Based Poly(Ester Urea Urethane) Nanoparticles as Carriers for Gambogic Acid and Effect on Cancer Cells. *J. Biomed. Mater. Res. Part A* **2017**, *105*, 475−490.
(30) Lu, W.; Wang, X.; Cheng, R.; Deng, C.; Meng, F.; Zhong, Z. Biocompatible and Bioreducible Micelles Fabricated from Novel α-Amino Acid-Based Poly(Disulfide Urethane)s: Design, Synthesis and Triggered Doxorubicin Release. *Polym. Chem.* **2015**, *6*, 6001−6010.
(31) Huang, F.; Cheng, R.; Meng, F.; Deng, C.; Zhong, Z. Micelles Based on Acid Degradable Poly(Acetal Urethane): Preparation, Ph-Sensitivity, and Triggered Intracellular Drug Release. *Biomacromolecules* **2015**, *16*, 2228−2236.
(32) Anantharaj, S.; Jayakannan, M. Melt Polycondensation Approach for Reduction Degradable Helical Polyester Based on L-Cystine. *J. Polym. Sci. Part A Polym. Chem.* **2016**, *54*, 2864−2875.
(33) Saxena, S.; Jayakannan, M. π-Conjugate Fluorophore-Tagged and Enzyme-Responsive l -Amino Acid Polymer Nanocarrier and Their Color-Tunable Intracellular FRET Probe in Cancer Cells. *Biomacromolecules* **2017**, *18*, 2594−2609.
(34) Saxena, S.; Pradeep, A.; Jayakannan, M. Enzyme-Responsive Theranostic FRET Probe Based on l -Aspartic Amphiphilic Polyester Nanoassemblies for Intracellular Bioimaging in Cancer Cells. *ACS Appl. Bio Mater.* **2019**, *2*, 5245−5262.
(35) Anantharaj, S.; Jayakannan, M. Amyloid-Like Hierarchical Helical Fibrils and Conformational Reversibility in Functional Polyesters Based on l-Amino Acids. *Biomacromolecules* **2015**, *16*, 1009−1020.
(36) Saxena, S.; Jayakannan, M. Development of L-Amino-Acid-Based Hydroxyl Functionalized Biodegradable Amphiphilic Polyesters and Their Drug Delivery Capabilities to Cancer Cells. *Biomacromolecules* **2020**, *21*, 171−187.
(37) Khuddus, M.; Jayakannan, M. Melt Polycondensation Strategy for Amide-Functionalized -Aspartic Acid Amphiphilic Polyester Nano-Assemblies and Enzyme-Responsive Drug Delivery in Cancer Cells. *Biomacromolecules* **2023**, *24* (6), 2643−2660.
(38) Joshi, D. C.; Saxena, S.; Jayakannan, M. Development of l -Lysine Based Biodegradable Polyurethanes and Their Dual-Responsive Amphiphilic Nanocarriers for Drug Delivery to Cancer Cells. *ACS Appl. Polym. Mater.* **2019**, *1*, 1866−1880.
(39) Anantharaj, S.; Jayakannan, M. Polymers from Amino Acids: Development of Dual Ester-Urethane Melt Condensation Approach and Mechanistic Aspects. *Biomacromolecules* **2012**, *13*, 2446−2455.
(40) Anantharaj, S.; Jayakannan, M. Catalysts and Temperature Driven Melt Polycondensation Reaction for Helical Poly(Ester-Urethane)s Based on Natural L-Amino Acids. *J. Polym. Sci. Part A Polym. Chem.* **2016**, *54*, 1065−1077.
(41) Aluri, R.; Jayakannan, M. One-Pot Two Polymers: ABB′ Melt Polycondensation for Linear Polyesters and Hyperbranched Poly-(Ester-Urethane)s Based on Natural l-Amino Acids. *Polym. Chem.* **2015**, *6*, 4641−4649.
(42) Chandra Joshi, D.; Ashokan, A.; Jayakannan, M. L -Amino Acid Based Phenol- and Catechol-Functionalized Poly(Ester-Urethane)s for Aromatic π-Interaction Driven Drug Stabilization and Their Enzyme-Responsive Delivery in Cancer Cells. *ACS Appl. Bio Mater.* **2022**, *5*, 5432−5444.
(43) Gavhane, U. A.; Joshi, D. C.; Jayakannan, M. Size- and Shape-controlled Biodegradable Polymer Brushes Based on l-Amino Acid for Intracellular Drug Delivery and Deep-Tissue Penetration. *Biomacromolecules* **2024**, *25* (6), 3756−3774.
(44) Chang, L.; Deng, L.; Wang, W.; Lv, Z.; Hu, F.; Dong, A.; Zhang, Z. Poly(ethyleneglycol)-b-poly(ε-caprolactone-co-γ-hydroxyl-ε- caprolactone) bearing pendant hydroxyl groups as nanocarriers for doxorubicin delivery. *Biomacromolecules* **2012**, *13*, 3301−3310.
(45) Hu, X.; Liu, S.; Chen, X.; Mo, G.; Xie, Z.; Jing, X. Biodegradable Amphiphilic Block Copolymer Bearing Protected Hydroxyl Groups: Synthesis and Characterization. *Biomacromolecules* **2008**, *9*, 553−560.
(46) Saulnier, B.; Ponsart, S.; Coudane, J.; Garreau, H.; Vert, M. Lactic Acid- Based Functionalized Polymers via Copolymerization and Chemical Modification. *Macromol. Biosci.* **2004**, *4*, 232−237.
(47) Sudo, A.; Sugita, S. A Highly Rigid Diamine Monomer Derived from Naturally Occurring myo-Inositol and its Use for Polymer Synthesis. *J. Polym. Sci., Part A: Polym. Chem.* **2016**, *54*, 3436−3443.
(48) Hahn, C.; Keul, H.; Möller, M. Hydroxyl-functional Polyurethanes and Polyesters: Synthesis, Properties and Potential Biomedical Application. *Polym. Int.* **2012**, *61*, 1048−1060.
(49) Begines, B.; Zamora, F.; Benito, E.; de Gracia Garcia-Martin, M.; Galbis, J. A. Conformationally Restricted Linear Polyurethanes

https://doi.org/10.1021/acspolymersau.4c00013
ACS Polym. Au 2024, 4, 392−404

from Acetalized Sugar-Based Monomers. *J. Polym. Sci., Part A: Polym. Chem.* **2012**, *50*, 4638−4646.
(50) Japu, C.; de Ilarduya, A. M.; Alla, A.; Jiang, Y.; Loos, K.; Muñoz-Guerra, S. Copolyesters Made from 1,4-Butanediol, Sebacic Acid, and D-Glucose by Melt and Enzymatic Polycondensation. *Biomacromolecules* **2015**, *16*, 868−879.

https://doi.org/10.1021/acspolymersau.4c00013
ACS Polym. Au 2024, 4, 392−404